J Mater Sci (2010) 45:888–896
DOI 10.1007/s10853-009-4016-4

Determination of the fibre orientation in composites using the structure tensor and local X-ray transform

M. Krause · J. M. Hausherr · B. Burgeth · C. Herrmann · W. Krenkel

Received: 28 August 2009 / Accepted: 2 November 2009 / Published online: 17 November 2009
© Springer Science+Business Media, LLC 2009

Abstract Computed tomography is a non-destructive testing technique based on X-ray absorption that permits the 3D-visualisation of materials at micron-range resolutions. In this article, computed tomography is used to investigate fibre orientation and fibre position in various fibre-reinforced materials such as ceramic matrix composites, glass fibre-reinforced plastics or reinforced concrete. The goal of this article is to determine the quantitative orientation of fibres in fibre-reinforced materials. For this purpose, a mathematical technique based on the structure tensor is used to determine the local orientation of fibres. The structure tensor is easy to implement and results in a fast algorithm relying solely on local properties of the given reconstruction. In addition, the local X-ray transform is used to denoise fibres and to segment them from the matrix.

Introduction

During the last decade, computed tomography (CT) has been developed as an efficient means of non-destructive testing in material sciences, see [1–5]. The resolution of CT is sufficient enough to determine the three-dimensional (3D) morphology of fibre-reinforced materials and to distinguish individual fibres. Nevertheless, there is still a lack of reliable algorithms to compute fibre orientation. The orientation of fibres is a very important characteristic of fibre-reinforced materials such as ceramic matrix composites (CMCs). This article serves two purposes. First of all, we present an algorithm for detecting the orientation of fibres and providing a quantitative distribution of the fibre orientation. Secondly, an algorithm for denoising and fibre segmentation is presented.

Related work

The use of CT as well as the use of scanning electron microscopy as methods for material characterisation is described in [6]. Both methods are explained in detail, each having its own advantages. Non-destructive testing techniques for CMC materials in general are explained in [7, 8]. A description of a practical reconstruction algorithm in CT is given in [9]. The mathematics of CT is explained in detail in [1, 10–12].

Examples of morphological applications using CT analysis are the detection and analysis of pores [13], crack distributions and the volumetric phase analysis. A further application is the determination of fibre orientation in fibre-reinforced materials as presented in Kastner et al. [14] and Robb et al. [15]. Kastner et al. first perform a segmentation between fibres and matrix followed by a skeletonisation algorithm. From the computed skeleton, the fibre's orientation can be computed. Robb et al. utilise a matched filter that adapts to the shape of a fibre to detect the fibre's orientation. This matched filter is an elongated anisotropic Gaussian. Algorithms to perform the necessary convolutions in an efficient way are described in [16]. Kastner et al. as well as Robb et al. perform an orientation tensor,

M. Krause (✉) · J. M. Hausherr · W. Krenkel
Ceramic Materials Engineering, University of Bayreuth, 95440 Bayreuth, Germany
e-mail: michael.krause@uni-bayreuth.de

J. M. Hausherr · C. Herrmann · W. Krenkel
Fraunhofer Projektgruppe Keramische Verbundstrukturen, Gottlieb-Keim-Straße, 95448 Bayreuth, Germany

B. Burgeth
Faculty of Mathematics and Computer Science, Saarland University, 66041 Saarbrücken, Germany

[17] that can be used to determine a local average orientation.

In this article, the structure tensor is used to determine the fibre's orientation. The structure tensor is described in detail in [18, 19]. This article follows Robb et al. by first computing the fibre's orientation in each fibre point. Then, the distribution of orientation vectors is visualised. In addition to visualising the distribution on a sphere, this article uses a simpler approach; by visualising the distribution on the x_1–x_2 plane and creating a graphical histogram of the distribution of the azimuth angle. This is preferable when the bigger part of all fibres is oriented in the x_1–x_2 plane.

In [20], the distribution of orientation vectors is weighted with the image intensity and with the degree of orientation tensor anisotropy, thus removing the need for prior fibre segmentation. The structure tensor is used by [21] to determine the axis of cylindrical objects, especially of C/C composite materials, as well as by [22] to perform 3D image skeletonisation.

For the purpose of fibre segmentation and anisotropic smoothing of fibres, this article contains an adaptation and modification of the local Radon transform, which is a 2D operator, described in [23], to the 3D case of short-fibre-reinforced materials.

Principles of computed tomography

Computed tomography is a non-destructive technique allowing the visualisation of the 3D internal structure of an object. The object is analysed by measuring its radiographs from different angles. In effect, a series of 2D radiographs of the object are generated while it is rotated around a central axis, each radiograph describing the absorption occuring at a specific angle. These individual radiograph images are then combined to a 3D model of the object by a mathematical process called reconstruction. This procedure is divided into two parts. The first part consists of a filtering step on the detector, reducing the effect of noise. The filtering step can be steered to a specific application, see [24]. The second part of the reconstruction process is the backprojection which backprojects the filtered radiographs onto a grid and sums up the contributions within the space covered by the projections, see [1].

Initially, CT has been developed as a tool for medical applications [25, 26]. However, in the last decade, it has been increasingly used for material testing as well [1]. The applications permit the analysis of almost any material with a spatial resolution down to ~ 1 µm. The results presented here were generated on a polychromatic X-ray CT-machine of the type HR-CT 150/03, located at the 'Fraunhofer Institut für Silicatforschung', Projektgruppe 'Keramische Verbundstrukturen' in Bayreuth/Germany.

Evaluation of CT scans

The focus lies on the analysis of fibre-reinforced materials, specifically the determination of fibre orientation in short-fibre-reinforced materials. As an example for such materials, the focus is on reinforced concrete, see Fig. 1. Human beings are able to recognise fibres in an intuitive and easy way, giving rise to a qualitative inspection of fibres. However, determination of quantitative results on fibre orientation in a justifiable amount of time is impossible, due to the presence of a large amount of fibres in the fibre-reinforced materials. In contrast to human beings, computers can handle large amounts of data reasonably fast, assuming the use of an efficient algorithm. In this article, a fast algorithm is presented, which does not rely on the distribution of *single fibres*, but on the distribution of local orientation of *single points* within a fibre. This algorithm, using the so-called structure tensor, is very stable in respect

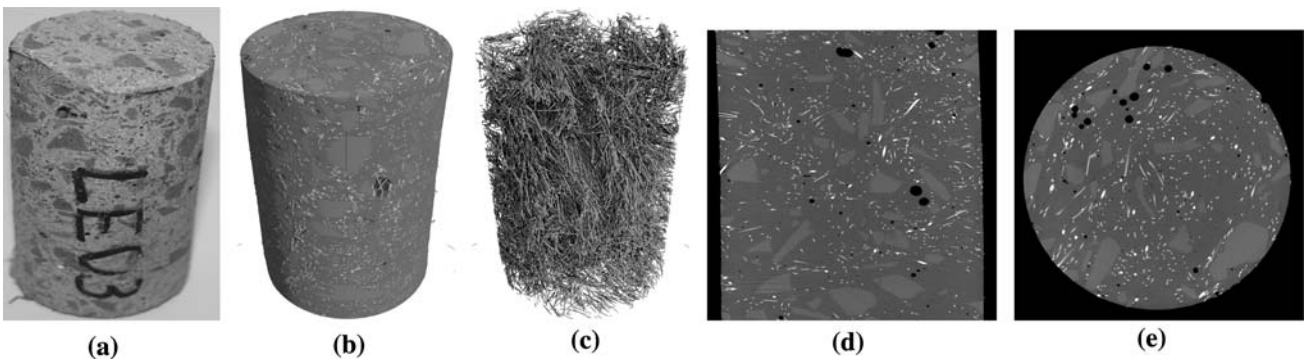

Fig. 1 Reinforced-concrete CT scan has been processed with VGStudio Max 2.0, **a** original, **b** CT scan, **c** extracted steel fibres, **d** slice along the cylinder axis, **e** slice perpendicular to the cylinder axis. One can distinguish between pores (*black*), concrete (*dark grey*), additives (*light grey*) and steel fibres (*white*)

of noise, as it computes an averaged version of the gradient. Based on the local orientation of each point x on a fibre, the fibre orientation distribution can be determined. Based on directional information, computed by the structure tensor, a second algorithm is applied to perform a segmentation between fibres and matrix. Finally, its effectiveness is evaluated using numerical examples.

Computing fibre orientation using the structure tensor

In order to calculate the fibre orientation, the structure tensor is introduced as a tool to determine fibre orientation, see [21]. The motivation for using the structure tensor as well as its most important properties are explained in the following.

Basic assumptions

We assume that a reconstruction based on a CT scan is given, such as the one shown in Fig. 1d, e. Figure 1d, e show two slices of Fig. 1b. The grey-value intensity of the reconstructed image can be described mathematically by a discrete function I. Furthermore, assume I to be the discrete version of a twice continuously differentiable function, so I can be integrated, differentiated and interpolated to its values at non-integers. If not stated otherwise, let a point x be a point on a fibre, assuming that a prior segmentation between fibres and matrix has been performed.

Characterisation of fibre orientation

Let $x \in \mathbb{R}^3$ be a fibre point. Because fibres are locally constant, a vector $v \in \mathbb{R}^3, |v| = 1$ exists, so that the difference quotient

$$(I(x+v) - I(x))^2 \approx 0. \tag{1}$$

Therefore, an orientation vector $w(x)$ can be specified by a minimisation criterion

$$w(x) = \operatorname{argmin}_{|v|=1} (I(x+v) - I(x))^2. \tag{2}$$

In order to find such an orientation vector $w(x)$ let at first v be unspecified. It is clear that for $w(x)$ has to hold $\nabla I(x)^\top w(x) \approx 0$. Then, a Taylor expansion is applied to (1) by using the gradient $\nabla I(x)$,

$$\begin{aligned}(I(x+v) - I(x))^2 &\approx (v^\top \nabla I(x))^2 \\ &= v^\top \nabla I(x) v^\top \nabla I(x) \\ &= v^\top \left(\nabla I(x) \nabla I(x)^\top \right) v.\end{aligned} \tag{3}$$

The latter equality holds because

$$v^\top \nabla I(x) = \nabla I(x)^\top v. \tag{4}$$

In order to compute an average gradient at point x, Eq. 3 is smoothed with a Gaussian K_{ρ_1},

$$K_{\rho_1} * ((I(\cdot + v) - I(\cdot))^2) \approx v^\top \left(K_{\rho_1} * \left(\nabla I \nabla I^\top \right) \right) v. \tag{5}$$

Note that the *sign* of the direction of ∇I is not important because $\nabla I \nabla I^\top$ is quadratic in ∇I. Only the *orientation* counts. Thus, no cancellation effects occur while computing the convolution. As the computation of gradients is ill posed, ∇I is replaced by a Gaussian derivative

$$\nabla I_\sigma(x) = \nabla (K_\sigma * I)(x) \tag{6}$$

which is a regularisation of the ill-posed problem of computing derivatives. It is worth mentioning that the Gaussian derivative ∇I_σ can be computed directly from tomographic data, see [27]. The additional Gaussian smoothing with K_{ρ_1} as performed in (5) is an additional regularisation. Equation 5 leads to the structure tensor J_{ρ_1} which is $\nabla I_\sigma \nabla I_\sigma^\top$ convolved component-wise with K_{ρ_1},

$$J_{\rho_1}(x) = K_{\rho_1} * \left(\nabla I_\sigma \nabla I_\sigma^\top \right)(x). \tag{7}$$

The Matrix $\nabla I_\sigma \nabla I_\sigma^\top$ is defined as

$$\nabla I_\sigma \nabla I_\sigma^\top = \begin{pmatrix} I_{x_1}^2 & I_{x_1} I_{x_2} & I_{x_1} I_{x_3} \\ I_{x_1} I_{x_2} & I_{x_2}^2 & I_{x_2} I_{x_3} \\ I_{x_1} I_{x_3} & I_{x_2} I_{x_3} & I_{x_3}^2 \end{pmatrix} \tag{8}$$

in respect of the partial derivatives I_{x_1}, I_{x_2} and I_{x_3} of I_σ. This way, a numerically stable approximation of $(I(x+v) - I(x))^2$ is obtained via the structure tensor,

$$K_{\rho_1} * (I(\cdot + v) - I(\cdot))^2 (x) \approx v^\top J_{\rho_1}(x) v \tag{9}$$

Therefore, the minimisation problem (2) can be approximated by its regularised form

$$w(x) = \operatorname{argmin}_{|v|=1} v^\top J_{\rho_1}(x) v. \tag{10}$$

The latter minimisation criterion is fulfilled by the eigenvector corresponding to the smallest eigenvalue [28] of $J_{\rho_1}(x)$. Thus, the orientation vector $w(x)$ can be obtained by solving an eigenvalue problem [29].

Properties of the structure tensor

In the previous section, it has been shown that an orientation vector $w(x)$ can be assigned to each fibre point, x, by means of the structure tensor. In this section, how the structure tensor can be used to distinguish between fibres and matrix is briefly described. First, the ability to compute an averaged version of the gradient is addressed. The direction, $g(x)$, that is most parallel to the gradient in the vicinity of a point x can be approximated by

$$g(x) = \operatorname{argmax}_{|v|=1} v^\top J_{\rho_1}(x) v. \tag{11}$$

Therefore, $g(x)$ is the eigenvector corresponding to the *largest* eigenvalue of $J_{\rho_1}(x)$, in contrast to the previous section, where the fibre orientation was given by the eigenvector corresponding to the *smallest* eigenvalue.

Speaking in general, the analysis of the eigenvalues $\lambda_1 \geq \lambda_2 \geq \lambda_3 > 0$ of the positive-definite tensor $J_{\rho_1}(x)$ can be used to describe the local characteristics of I in the vicinity of x, see [22]:

- $\lambda_1 \approx \lambda_2 \approx \lambda_3 > 0$ indicates isotropy.
- If $\lambda_1 \gg \lambda_2 \approx \lambda_3 > 0$, then the point, x, is part of a planar structure in I. No favoured fibre direction exists, but two eigenvectors that span a plane that contains x do.
- If $\lambda_1 \approx \lambda_2 \gg \lambda_3 > 0$, then the point x is part of a line, which means that x is a fibre point. As already stated, the eigenvector corresponding to λ_3 describes the fibre's orientation.

Therefore, fibres should satisfy $\lambda_1 \approx \lambda_2 \gg \lambda_3 > 0$.

Fibre segmentation and anisotropic smoothing of fibres

If fibre orientation is not uniform (see Sect. 6.3.2), then a restriction to the orientation vectors of fibre points can be beneficial. Therefore, a segmentation between fibres and matrix might be necessary. In this section, an adaptation to the 3D case of the 2D concepts proposed in [23] is performed. In [23], the local Radon transform is used to segment retinal vessels from non-vessel points. In order to perform this segmentation, a strongly anisotropic kernel is rotated and convolved with the image. The kernel is chosen as a line detector. The maximum response in respect of the direction of the kernel is chosen as a result, and a threshold is applied. This algorithm is a brute-force algorithm. In the 3D case, this approach would take too much time, requiring the computation of a large number of convolutions, and so the fibre orientation has to be computed prior to segmentation using the structure tensor. This way, only one convolution must be computed at each point x.

Local coordinates

The proposed fibre-detection algorithm is based on the convolution with a kernel that is elongated in direction $w(x)$. Let the vector, $w(x)$, be denoted as ω which can be written in spherical coordinates $(\theta, \varphi) \in [0°, 360°) \times [-90°, 90°]$ as

$$\omega = \omega(\theta, \varphi) = \begin{pmatrix} \cos\theta\cos\varphi \\ \sin\theta\cos\varphi \\ \sin\varphi \end{pmatrix}. \tag{12}$$

An orthonormal base of $\mathbb{R}^3$ that fits to the fibre orientation, is given by $\omega = \omega(\theta, \varphi)$, $\omega_1^\perp = \omega_1^\perp(\theta + 90°, 0°)$ and $\omega_2^\perp = \omega_2^\perp(\theta, \varphi + 90°)$. The new base can be obtained by a rotation of the vectors of the standard base $\{e_1, e_2, e_3\}$ by φ around the x_2-axis followed by a rotation by the angle θ around the x_3-axis. The vectors $\{\omega, \omega_1^\perp, \omega_2^\perp\}$ will be used in the discretisations in the following sections.

The local X-ray transform

The standard X-ray transform, P, can be used as a model in 3D CT [10]. It maps an object I to its integrals over lines,

$$PI(\omega, b) = \int_{\mathbb{R}} I(b + t\omega)\mathrm{d}t, \tag{13}$$

where ω is the direction of the line, and $b \in \omega^\perp$ is perpendicular to ω. As this article aims for the local analysis of fibres through a fibre point, x, it is beneficial to introduce a new coordinate system. Let a point p be $p = x + t\omega + b$, where ω is the direction of the fibre, $b = u_1\omega_1^\perp + u_2\omega_2^\perp$ is a shift vector perpendicular to ω and $x + t\omega$ describes the nearest point from p on the fibre. The shift b will be used later on to compute the Laplacian in the plane perpendicular to ω containing the point $x + t\omega$. As the image intensity I is degraded by noise, a regularisation is necessary. This regularisation is achieved by the local X-ray transform.

$$P_L I(x, \omega, b) = \int_{\mathbb{R}} K_{\rho_2}(t) I(x + t\omega + b)\mathrm{d}t. \tag{14}$$

The integration weight K_{ρ_2} is a Gaussian with centre zero and standard deviation ρ_2. It also serves as a localised version of (13), which is preferable, as it is not aimed towards the computation of properties of I from non-local data.

Smoothing of the input image

The integral (14) is a type of linear but anisotropic diffusion, the direction of diffusion is the direction of the fibre. Therefore, anisotropic Gaussian smoothing by the computation of line integrals of the image while preserving fibres is possible.

Fibre segmentation

In [23], the second derivative of the local Radon transform has been used to detect retinal vessels. In this article, the local Radon transform is replaced by the 3D local X-ray transform. The computation of the second derivative is realised by a Laplacian with respect to the shift vector b,

$$\Delta_b P_L I(x,\omega,b) = \Delta_b \int_{\mathbb{R}} K_{\rho_2}(t) I(x + t\omega + b)\mathrm{d}t. \tag{15}$$

As fibres are assumed to be darker than the background, it is reasonable that at fibre points, $x + t\omega$, the response of the above integral is greater than zero. If the fibres are brighter than the matrix, then the image is inverted. In addition, a criterion for the segmentation of fibres is

$$\Delta_b P_L I(x,\omega,0) > T \tag{16}$$

for a suitable chosen threshold T. Numerical examples show that, for some examples, it is possible to choose Otsu's threshold [30] which is computed from the image histogram without requiring human interaction.

Efficient implementation

The local X-ray transform is approximated by the trapezoid rule

$$P_L I(x,\omega,b) \approx \sum_{k\in\mathbb{Z}} K_{\rho_2}(k) I(x + k\omega + b), \tag{17}$$

and therefore, is sampled with step size one. As ω is mostly not parallel to the Cartesian grid, I is not known on all points that are needed to evaluate (17). Therefore, I is interpolated trilinear leading to a formula of the form

$$P_L I(x,\omega,b) \approx \sum_{m\in\mathbb{Z}^3} \alpha_{\omega,b}(m) I(x + m). \tag{18}$$

Writing b in the $\{\omega_1^\perp, \omega_2^\perp\}$-coordinate system, a standard discretisation of the derivative in (16) is

$$\begin{aligned}\Delta_b P_L I(x,\omega,0) \approx &-4 \cdot P_L I(x,\omega,0)\\ &+ P_L I(x,\omega,\omega_1^\perp) + P_L I(x,\omega,-\omega_1^\perp)\\ &+ P_L I(x,\omega,\omega_2^\perp) + P_L I(x,\omega,-\omega_2^\perp).\end{aligned} \tag{19}$$

As $\omega_1^\perp$ and $\omega_2^\perp$ uniquely depend on ω, this in combination with (18), leads to an approximation of the form

$$\Delta_b P_L I(x,\omega,0) \approx \sum_{m\in\mathbb{Z}^3} \beta_\omega(m) I(x + m). \tag{20}$$

Since the filters β_ω are sparse, the correlation (20) is highly efficient. Note that β_ω can be pre-computed in a sufficiently dense discrete subset $\{\omega_i\}_{i=1,\ldots,p}$ of the unit sphere $\mathcal{S}^2$ of $\mathbb{R}^3$. Thus, the explicit interpolation of I in $\mathbb{R}^3$ as performed in (18) can be avoided. Choosing one ω_i instead of $\omega = w(x)$ (e.g. through the nearest neighbour interpolation) requires the computation of only one correlation with a *precomputed* kernel per point x, thereby avoiding the performance of the necessary interpolations in $\mathbb{R}^3$ explicitly. Therefore, for each point, x, only one line integral has to be approximated. The same efficient behaviour holds for the smoothing of the image I in Sect. 5.3 since $P_L I(x,\omega,0)$ can be approximated by a formula of the form

$$P_L I(x,\omega,0) \approx \sum_{m\in\mathbb{Z}^3} \gamma_\omega(m) I(x + m) \tag{21}$$

with filters γ_ω that are even sparser than the filters β_ω.

Note, that the filters β_ω and γ_ω are symmetrical with respect to the origin. Therefore, the involved correlations are, in fact, also convolutions.

Numerical examples

Proving the non-specific use of any material type, the presented algorithms are evaluated on CT images of different materials. In order to start with, the use of the local X-ray transform for anisotropic image smoothing and for fibre segmentation is shown. Then, the ability of the structure tensor to determine fibre orientation is presented on short-fibre-reinforced concrete. Next, two types of carbon-fibre-reinforced silicon carbide composites (C/SiC) are examined, one being a 0°/90° woven fabric and the other a short-fibre-reinforced (5-mm) C/SiC. In both cases, the fibre volume content is 50–55%.

Image denoising and fibre segmentation

The local X-ray transform can be used as a tool for denoising the original Fig. 2a, see Fig. 2b. In order to improve the results, a linear isotropic diffusion for a small amount of time has been applied. The diffusion process via the local X-ray transform is linear, but anisotropic. Whereas the background is smoothed strongly, the fibres are still segmented from the matrix. Another aspect of the local Radon transform, namely its ability to be used for segmentation is shown in Fig. 2d which is a thresholded version of Fig. 2c

Short-fibre-reinforced concrete

The theoretic results have been evaluated at a small section of Fig. 1b. The parameter values for the computation of the structure tensor $J_{\rho_1} = K_{\rho_1} * (\nabla I_\sigma \nabla I_\sigma^\top)$ are $\sigma = 0.65$ and $\rho_1 = 4$.

Figure 3a shows the front side of a spherical representation of the orientation vectors. In order to compute fibre orientation instead of fibre direction, the x_3-component has to be positive. If the x_3 component is negative, then the orientation vector is multiplied with -1. Note that only points x with value of $I(x)$ greater than the threshold $T = 245$ are regarded as fibre points. All other points are not processed.

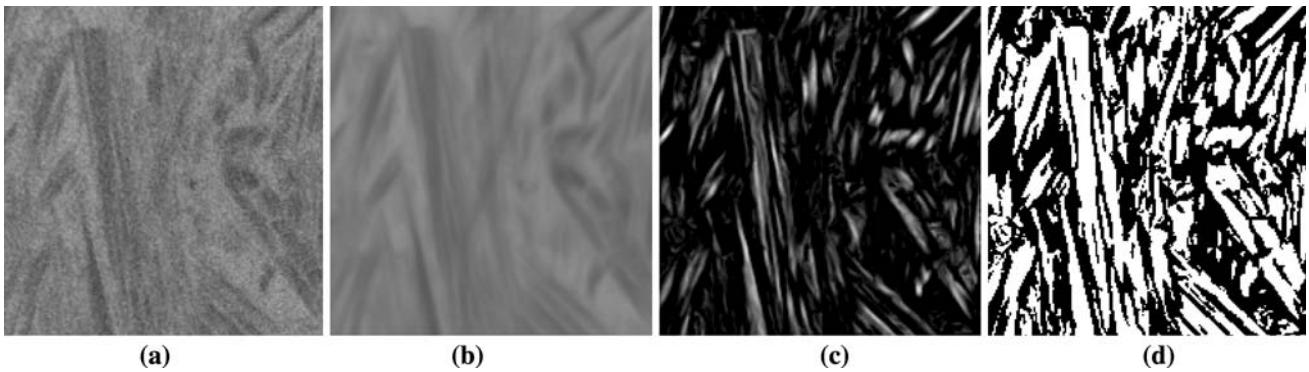

Fig. 2 Application of local X-ray transform P_L on a small section of short-fibre-reinforced C/SiC, **a** slice of the original image, **b** linear but anisotropic diffusion, **c** application of $\Delta_b P_L$ on **a** and **d** final segmentation

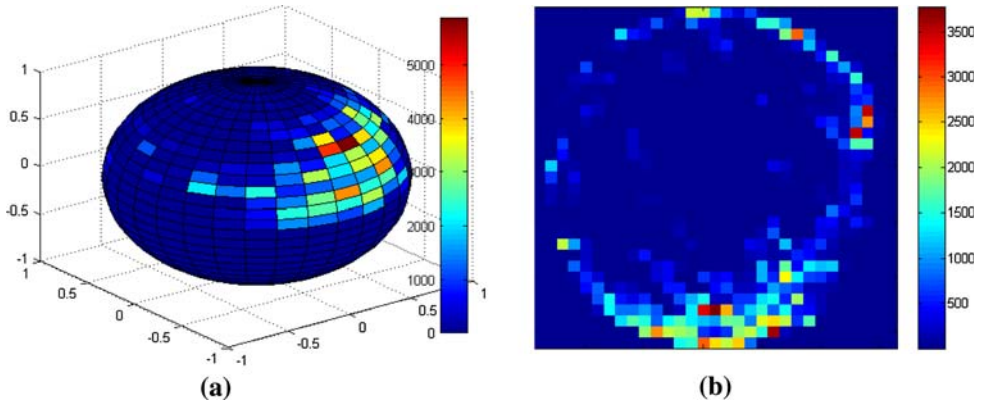

Fig. 3 Global distribution of orientation vectors of short-fibre-reinforced concrete. **a** Visualisation on a sphere, the number of orientation vectors pointing to a cell of the sphere has been counted. Red indicates a high number of vectors whereas blue indicates no vectors. This is a statistical approach, because only the global distribution of fibre orientation has been computed. **b** Each orientation vector $w(x)$ at the point x of the section has been projected on the x_1–x_2-plane. The x_1–x_2 plane has been divided in 31 × 31 cells, and the number of orientation vectors projected on a cell has been counted

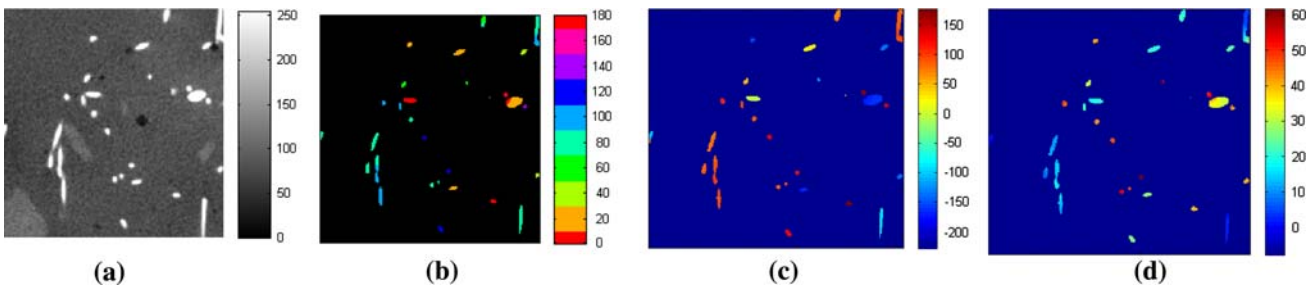

Fig. 4 Results on reinforced concrete: one slice is shown, **a** slice of the original image, **b** azimuth and elevation encoded in one colour, **c** azimuth angle of orientation vectors and **d** elevation angle of orientation vectors

Figure 3b shows a representation of the distribution of the orientation vectors projected to the x_1–x_2 plane.

Figure 4a shows a slice of the original 3D image I. Figure 4b shows a representation of the orientation vectors that both encodes azimuth and elevation in one colour. The azimuth is shown in the colourbar on the right, and the elevation is described by the brightness.

The regions between the fibres have been depicted in dark blue or black. Fig. 4c, d show the azimuth and elevation, respectively.

Silicon carbide composites

In this section, the proposed algorithms are evaluated on C/SiC material, on fabric and on short-fibre-reinforced

C/SiC. The CMCs are manufactured using the Liquid Silicon Infiltration (LSI) process, and is composed of an HTA fabric (3K) with a matrix of SiC. The short-fibre C/SiC contains chopped HTA fibre bundles of approximately 5-mm length. The fibre volume content is 50−55% in both cases.

Fabric-reinforced C/SiC

Figure 5a, b show the orientation vector distribution on a fabric reinforced C/SiC. The fibre bundle's orientation is bidirectional in 0° and 90° orientation. It can be easily verified that two orientations dominate. All the points have been processed, regardless of whether they are fibre points or not. This means that the threshold, T, has been set to zero.

Figure 5c shows the original CT-image slice. Owing to the Gaussian smoothing with a standard deviation of $\rho_1 = 2$ in computing the structure tensor, and to the small distance between different fibres, the orientation is propagated from fibres to the matrix, and vice versa. Therefore, the computed orientation vector at a point x is almost constant in a vicinity of x (at least modulo 180°) as can be seen from Fig. 5d. The individual sectors of the fabric are clearly visible. Figure 5d visualises the horizontal fibre orientation in one slice of the fabric. Since it is required that the choice of normalising the x_3-component of the orientation vectors be positive, the different ondulations of the fabric results in two different colours in each sector (yellow–dark blue red), (light blue–orange). Each colour also encodes the fact whether the fabric is woven in direction of the positive or the negative x_3-axis.

Short-fibre-reinforced C/SiC

Figure 6 shows the fibre orientation distribution on short-fibre-reinforced C/SiC. In order to improve the results, a segmentation between fibres and matrix using the Laplacian of the local X-ray transform has been applied, see Fig. 2c. This means that for the statistics shown in Fig. 6a, b only fibre points have been taken into account. The standard deviation in computing the structure tensor was $\rho_1 = 2$ and that used for the computation of the local X-ray transform was $\rho_2 = 4$. It can be seen that the fibres are anisotropic but located in the x_1–x_2 plane. Figure 6c shows the distribution of the azimuth on the whole imagestack.

Figure 7b, c show the azimuth and the elevation for one slice of the original image, see Fig. 7a.

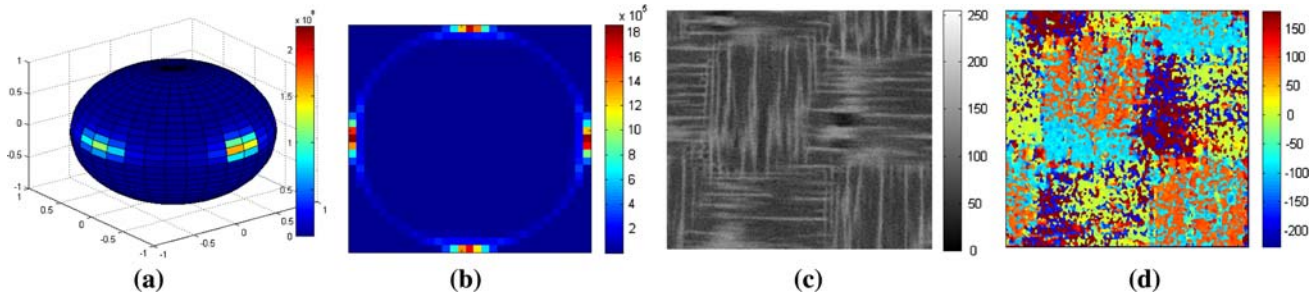

Fig. 5 Results of structure tensor on fabric reinforced C/SiC, **a** distribution on a sphere, **b** distribution of orientation vectors projected to the x_1–x_2 plane, **c** slice of the original image and **d** azimuth angle of orientation vectors in slice

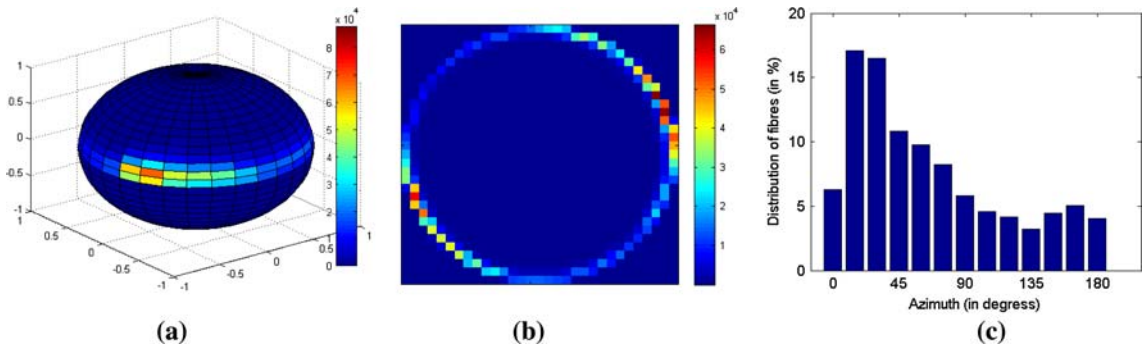

Fig. 6 Global distribution of orientation vectors of short-fibre-reinforced C/SiC, **a** distribution on a sphere, **b** distribution of orientation vectors projected to the x_1–x_2 plane and **c** distribution of azimuth

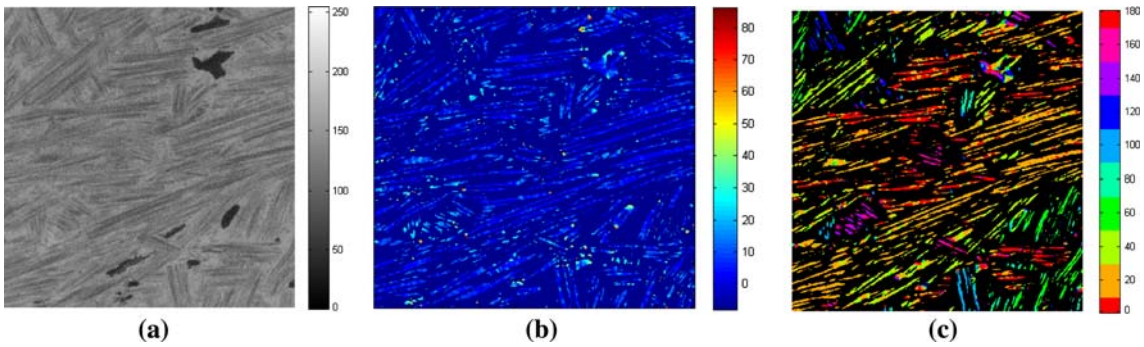

Fig. 7 Results of structure tensor on short-fibre-reinforced C/SiC, **a** slice of the original image, **b** elevation angle of orientation vectors and **c** azimuth angle of orientation vectors

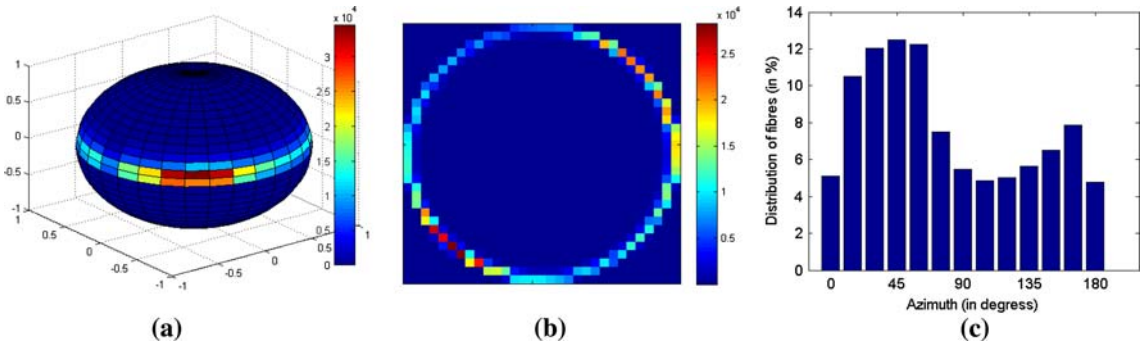

Fig. 8 Global distribution of orientation vectors of glass fibre-reinforced plastics, **a** distribution on a sphere, **b** distribution of orientation vectors projected to the x_1-x_2 plane and **c** distribution of azimuth

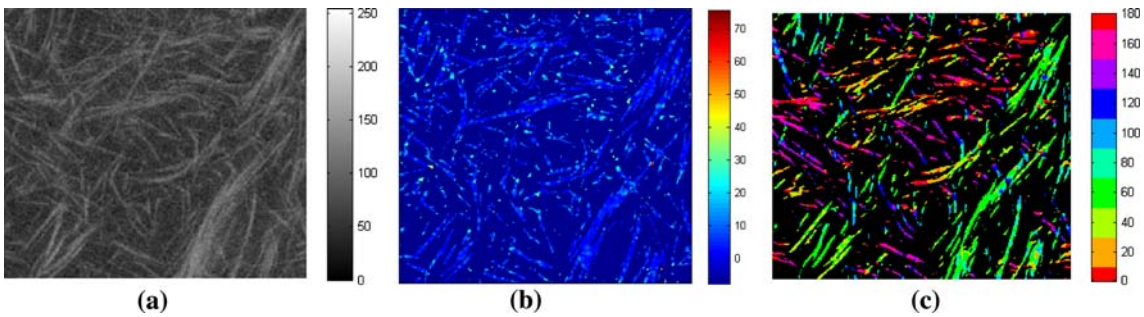

Fig. 9 Results of structure tensor on glass fibre-reinforced plastics, **a** slice of the original image, brightened and contrast-enhanced, **b** elevation angle of orientation vectors and **c** azimuth angle of orientation vectors

Glass fibre-reinforced plastics

Figure 8 shows the distribution of orientation vectors as well as the global distribution of the azimuth on glass fibre-reinforced plastics [31]. The orientation vectors are mostly oriented in the x_1–x_2 plane with a peak 45° of in the x_1–x_2 plane.

Figure 9 shows the results in one slice. The segmentation between fibres and matrix has been performed with the Laplacian of the local X-ray transform as has been done for short-fibre-reinforced C/SiC. In addition, the method can be used to determine the fibre-volume content by binarisation.

Conclusions

In this article, a method for computing the quantitative fibre orientation distribution has been presented. This method is based on the structure tensor, which computes

the average gradient direction in the vicinity of a point x. In addition, the structure tensor can be used to compute a direction in which the image information is constant, if such a direction exists. This leads to the computation of fibre orientation. If the fibres are locally oriented in one direction, then no prior segmentation between fibres and matrix is needed; however, if the fibres are oriented randomly, an a priori segmentation can be beneficial. In the case of short-fibre-reinforced concrete; the segmentation can be performed easily on the input image, because the X-ray attenuation coefficient of steel is much higher than that of concrete. Therefore, the segmentation can be based on the grey value of the CT image. If a segmentation using the grey value is too demanding, then a contrast enhancement by a Laplacian operator perpendicular to the fibre orientation is preferable. For homogenious material such as fabric, the structure tensor is the ideal means of determining fibre orientation distribution.

Acknowledgements The authors gratefully acknowledge the support of the 'Bayrische Forschungsstiftung' (BFS) for funding this research in respect of the project 'Kontisilizierung' (Förderkennzeichen AZ-719-06).

References

1. Stock SR (2009) Micro computed tomography. CRC Press, Boca Raton, Fl
2. Buffiére JY, Maire E, Cloetens P, Lormand G, Fougeres R (1999) Acta Mater 47:1613
3. Buffière JY, Savelli S, Maire E (2000) Characterisation of MMC_p and cast aluminium alloys. X-ray tomography in materials science. Hermes Science Publications, Paris, pp 103–114
4. Martín-Herrero J, Germain C (2007) Carbon 45:1242
5. Babout L, Marrow TJ, Engelberg D, Withers PJ (2006) Mater Sci Techol 22(9):1068
6. Hausherr JM, Fischer F, Krenkel W, Altstädt V (2006) In: Proceedings of conference on damage in composite material, Stuttgart. http://www.ndt.net/article/cdcm2006/papers/hausherr.pdf. Accessed 24 Aug 2009
7. Hausherr J, Krenkel W (2008) Ceramics matrix composites. Wiley VCH, Weinheim, pp 261–286
8. Herrmann C, Hausherr JM, Krenkel W (2009) In: Verbundwerkstoffe, Wiley VCH, New York, pp 249–256
9. Feldkamp LA, Davis LC, Kress JW (1984) J Opt Soc Am 1(6): 612
10. Natterer F (1986) The mathematics of computerized tomography. Teubner, Wiley, Stuttgart, Chichester
11. Natterer F, Wübbeling F (2001) Mathematical methods in image reconstruction. SIAM, Philadelphia, PA
12. Kak AC, Slaney M (2001) Principles of computerized tomographic imaging. SIAM, Roberto'Malley, USA
13. Hausherr JM, Meinhardt J, Hassink B, Herrmann C, Daimer J, Raether G, Krenkel W (2009) In: Proceedings of 11th international conference on European ceramic society, ECERS, Krakow
14. Kastner J, Pfeifer F, Heinzl C, Freytag R (2008) In: DACH-Jahrestagung 2008 in St. Gallen, http://www.ndt.net/article/dgzfp2008/Inhalt/di3a1.pdf. Accessed 26 Aug 2009
15. Robb K, Wirjadi O, Schladitz K (2007) In: HIS, pp 320–325
16. Lampert CH, Wirjadi O (2006) IEEE Trans Image Process 15(11):3501
17. Knutsson H (1989) In: The 6th Scandinavian conference on image analysis, Oulu, Finland, p 244, Report LiTH-ISY-I-1019, Computer Vision Laboratory, Linköping University, Sweden
18. Van Ginkel M (2002) Image analysis using orientation space based on steerable filters, Delft University of Technology, PhD thesis
19. Van Kempen GMP, van den Brink N, van Vliet LJ, Van Ginkel M, Verbeek PW, Blonk H (1999) In: Proceedings of the 11th Scandinavian conference on image analysis SCIA'99, Kangerlussuaq, Greenland, pp 447–455
20. Axelsson M (2008) In: ICPR, IEEE, pp 1–4
21. Mulat C, Donias M, Baylou P, Vignoles G, Germain C (2008) J Electron Imaging 17:031108
22. Zeyun Y, Bajaj C (2006) In: IEEE international conference on image processing, pp 2513–2516
23. Krause M, Alles RM, Burgeth B, Weickert J (2008) Retinal vessel detection via second derivative of local radon transform. Universität des Saarlandes Technical Report No. 212. http://www.math.uni-sb.de/service/preprints/preprint212.pdf. Accessed 28 Oct 2009
24. Louis AK (1996) Inverse Probl 12:175
25. Cormack AM (1963) J Appl Phys 34:2722
26. Hounsfield GN (1973) Computerized transverse axial scanning (tomography): part 1. description of system. Br J Radiol 46:1016
27. Louis AK (2009) Inverse problems and imaging. http://www.num.uni-sb.de/iam/veroeffentlichungen. Accessed 27 Aug 2009
28. Fischer G (2005) Lineare algebra. Vieweg+Teubner, Wiesbaden
29. Deuflhard P (2002) Numerische Mathematik 1. Gruyter, Berlin
30. Otsu N (1979) IEEE Trans Syst Man Cybernet 9(1):62
31. Rohde M, Fischer F, Altstädt V, Herrmann C, Krenkel W, Hausherr JM (2009) IMC-Spritzgiesscompounder-Potentiale der Langfaserverstärkung. In: Verbundwerkstoffe, Wiley, VCH, New York, pp 483–66